ıal Research Laboratory
ıgton, DC 20375-5000

NRL Memorandum Report 6914

Theory of Electromagnetic Instability of an Intense Beam in a Quadrupole Focusing System

CHA-MEI TANG, J. KRALL AND T. SWYDEN*

Beam Physics Branch
Plasma Physics Division

**FM Technologies, Inc.*
Fairfax, VA

February 18, 1992

REPORT DOCUMENTATION PAGE

Form Approved
OMB No 0704-0188

1. AGENCY USE ONLY (Leave blank)	2. REPORT DATE	3. REPORT TYPE AND DATES COVERED
	February 18, 1992	Interim

4. TITLE AND SUBTITLE

Theory of Electromagnetic Instability of an Intense Beam in a Quadrupole Focusing System

5. FUNDING NUMBERS

ARPA Order 7781

6. AUTHOR(S)

Cha-Mei Tang, J. Krall and T. Sywden*

7. PERFORMING ORGANIZATION NAME(S) AND ADDRESS(ES)

NRL
Washington, DC 20375-5000

8. PERFORMING ORGANIZATION REPORT NUMBER

NRL Memorandum Report 6914

9. SPONSORING/MONITORING AGENCY NAME(S) AND ADDRESS(ES)

DARPA
Arlington, VA 22203

NSWC
Silver Spring, MD 20903

ONR
Arlington, VA 22217

10. SPONSORING/MONITORING AGENCY REPORT NUMBER

11. SUPPLEMENTARY NOTES

*FM Technologies, Inc., Fairfax, VA

12a. DISTRIBUTION/AVAILABILITY STATEMENT

Approved for public release; distribution unlimited.

12b. DISTRIBUTION CODE

13. ABSTRACT *(Maximum 200 words)*

Discrete quadrupole focusing systems are subject to an electromagnetic instability wherein the growing transverse motion of the beam interacts with the quadrupole field and the TE_{11} waveguide mode. The dispersion relation is derived, which is a matrix equation of infinite dimensions. We show that an appropriately truncated matrix equation is able to give exact growth rates. Furthermore, analytical growth rates are obtained and instability boundaries are established. Numerical solutions of the dispersion relation show that the overall stability properties are not favorable for long pulse, high-current electron beams. The stability properties of ion beams are also discussed.

14. SUBJECT TERMS	15. NUMBER OF PAGES
3 wave instability discrete quadrupole focusing systems	32
	16. PRICE CODE

17. SECURITY CLASSIFICATION OF REPORT	18. SECURITY CLASSIFICATION OF THIS PAGE	19. SECURITY CLASSIFICATION OF ABSTRACT	20. LIMITATION OF ABSTRACT
UNCLASSIFIED	UNCLASSIFIED	UNCLASSIFIED	UL

CONTENTS

I. INTRODUCTION 1

II. DISPERSION RELATION 3

III. ANALYTICAL BEAM LINE DECOMPOSITION 8

IV. ANALYTICAL EXPRESSIONS FOR GROWTH RATES AND GROUP VELOCITY 10

V. NUMERICAL EXAMPLES 13

VI. SUMMARY AND COMMENTS 16

ACKNOWLEDGMENTS 16

APPENDIX A 17

REFERENCES 18

THEORY OF ELECTROMAGNETIC INSTABILITY OF AN INTENSE BEAM IN A QUADRUPOLE FOCUSING SYSTEM

I. Introduction

Discrete quadrupole focusing systems, also called FODO lattices, have been used to transport charged particle beams for a variety of applications. A FODO lattice is an alternative to helical quadrupole windings for strong focusing. Helical quadrupole (stellarator) focusing systems have been found to be subject to an electromagnetic instability, which we referred to as the three-wave instability.[1-3] This has been observed experimentally for a 325 A, 950 keV beam with an 80 nsec pulse length.[4] In that case, the stellarator gradient was 400 G/cm, the stellarator pitch length was 18 cm, and the axial magnetic field was 1.2 kG. The growth of the instability and subsequent beam loss was accompanied by 3 GHz radiation, as predicted by theory.

Here, we consider the corresponding instability for transverse perturbations of a beam centroid interacting with a FODO lattice field and a TE_{11} waveguide mode. The advantages of using FODO lattices are: (i) variations in periodicity are easily introduced, (ii) variations in periodicity can change the character of electromagnetic instability and reduce the overall growth rate, (iii) lower growth rates in some regimes and (iv) preliminary particle simulations show saturation at low values. Even though the FODO lattice lacks a stable regime, the small growth rates may allow a cure by any one of several methods, such as loss in the waveguide.

The dispersion relation may be solved in the usual way, with the growth rates being the imaginary parts of the roots of the determinant of a dispersion matrix. Due to the periodicity of the FODO lattice, however, the dispersion matrix is of infinite dimension. This instability[5,6] was recently analyzed via Floquet theory[5] and via approximate dispersion relations based on two different approaches.[5,6] In this paper, we derive the dispersion

Manuscript approved November 5, 1991.

relation and show that the exact growth rate, in agreement with the results from Floquet theory, can be obtained from a truncated dispersion matrix. Furthermore, we are able to approximately factor a zeroth-order form of the dispersion relation to find all the beam modes. Identifying the beam mode that causes the instability, we are able to derive analytic expressions for the growth rates and establish various regions of instability.

II. Dispersion Relation

We consider an alternating gradient quadrupole field (B_{qx}, B_{qy}), where

$$B_{qx} = -B_q k_q f(z) y, \qquad B_{qy} = -B_q k_q f(z) x, \tag{1a-b}$$

$B_q k_q$ is the peak quadrupole field, $f(z)$ is periodic, $k_q = 2\pi/\lambda_q$ and λ_q is the period of the quadrupole field. The representation for the quadrupole field in Eqs. (1a-b) is valid near the z-axis, i.e., $(x^2 + y^2)^{1/2} << \lambda_q/2\pi$.

In equilibrium, the electron beam travels along the axis of a perfectly conducting circular waveguide of radius r_g at velocity v_o and is monoenergetic with $\gamma_o = (1-\beta_o^2)^{-1/2}$, where $\beta_o = v_o/c$. Both the beam radius and beam centroid displacement are assumed to be small in comparison to the waveguide radius. We include induced image charges and currents due to the displaced beam. The induced electric and magnetic fields near the z-axis are

$$\mathbf{E}_{ind} = -2\frac{m_o c^2}{e}\frac{\nu}{r_g^2}(x_c \hat{\mathbf{e}}_x + y_c \hat{\mathbf{e}}_y), \tag{2a}$$

$$\mathbf{B}_{ind} = 2\frac{m_o c^2}{e}\frac{\nu}{r_g^2}\beta_o(y_c \hat{\mathbf{e}}_x - x_c \hat{\mathbf{e}}_y), \tag{2b}$$

where $x_c(z_o, z) = x_c(z_o, t = (z-z_o)/v_o)$ and $y_c(z_o, z) = y_c(z_o, t = (z-z_o)/v_o)$ are the beam centroid coordinates, $\nu = \omega_b^2 r_b^2/4c^2$ is Budker's parameter, ($\nu \simeq |I_e|/17\beta$ for an electron beam where I_e is the electron beam current in units of kilo-Amperes), $\omega_b^2 = 4\pi e^2 n_e/m_o$, n_e is the electron density, m_o is the electron mass e is the elementary charge (assumed positive), r_b is the beam radius and z_o is the axial position of the electron at $t = 0$.

We expect the TE_{11} mode to have the largest growth rate because its electric field peaks on axis. It vector potential can be written as

$$\begin{aligned} \mathbf{A} &= [A_x(r,\theta,z)\hat{\mathbf{e}}_x + A_y(r,\theta,z)\hat{\mathbf{e}}_y]\, e^{-i\omega t} + c.c. \\ &= [\mathbf{A}_+(r,\theta,z) + \mathbf{A}_-(r,\theta,z)]\, e^{-i\omega t} + c.c., \end{aligned} \tag{3}$$

where

$$\mathbf{A}_\pm(r,\theta,z) = \int dk_\pm b_{\pm 11}(k_\pm)\left[J_o(\mu_{11} r)\hat{\mathbf{e}}_\pm + J_2(\mu_{11} r)e^{\pm i2\theta}\hat{\mathbf{e}}_\mp\right] e^{ik_\pm z},$$

$\mathbf{A}_\pm$ are complex amplitudes associated with the (+) right-handed circularly polarized (RHCP) wave and (−) left-handed circularly polarized (LHCP) wave, J_n is the n_{th} order Bessel function, $b_{\pm 11}$ are complex constants, ω is the radian frequency, $k_\pm$ are the wave numbers associated with the RHCP and LHCP waves, $\hat{\mathbf{e}}_\pm = (\hat{\mathbf{e}}_x \pm i\hat{\mathbf{e}}_y)/2$ and c.c. denotes the complex conjugate. The boundary condition, requiring the tangential component of the electric field to vanish on the perfectly conducting waveguide surface, gives the condition $J_1'(r = \mu_{11} r_g) = 0$, where $\mu_{11} r_g$ is the the largest positive zeroth of Bessel function J_1' and $'$ denotes d/dr.

The wave equation for $\mathbf{A}$ is given by

$$\left(\nabla_\perp^2 + \frac{\partial^2}{\partial z^2} - \frac{1}{c^2}\frac{\partial^2}{\partial t^2}\right)\mathbf{A} = -\frac{4\pi}{c}\mathbf{J}_c, \tag{4}$$

where $\nabla_\perp^2 \equiv \nabla^2 - \frac{\partial}{\partial z}$ is the transverse Laplacian, and $\mathbf{J}_c = -en_e\pi r_b^2 \mathbf{v}_c$ is the macroscopic transverse current associated with the beam centroid. Assuming that the particle motion is driven by field on axis, the current can be written as

$$\mathbf{J}_c = -\nu\frac{m_o c^2}{e}\delta(x)\delta(y)\left(\frac{dx_c}{dt}\hat{\mathbf{e}}_x + \frac{dy_c}{dt}\hat{\mathbf{e}}_y\right), \tag{5}$$

where $[x_c(z,t), y_c(z,t)]$ are the coordinates of beam centroid.

The wave equation can be rewritten as

$$L\left[(a_x \pm i a_y)e^{-i\omega t} + c.c\right] = -4\pi\frac{\nu}{c}\delta(x)\delta(y)\frac{d}{dt}(x_c \pm i y_c), \tag{6}$$

where $a_{x,y} = (e/m_o c^2)A_{x,y}$ and $L = \nabla_\perp^2 + \partial^2/\partial z^2 + \omega^2/c^2$.

The vector potential in (6) has the form

$$\begin{aligned}(a_x \pm i a_y)e^{-i\omega t} =& \frac{e}{m_o c^2}\int dk_\mp b_{\mp 11}(k_\mp) J_o(\mu_{11} r) e^{i(k_\mp z - \omega t)} \\ &+ \frac{e}{m_o c^2}\int dk_\pm b_{\pm 11}(k_\pm) J_2(\mu_{11} r) e^{\pm i2\theta} e^{i(k_\pm z - \omega t)}\end{aligned} \tag{7}$$

After L operated on the normalized vector potential, Eq. (6) can be written as

$$\frac{e}{m_o c^2}e^{-i\omega t}\left[\int dk_\mp e^{ik_\mp z}\left(\frac{\omega^2}{c^2} - k_\mp^2 - \mu_{11}^2\right) J_o(\mu_{11} r) b_{\mp 11}(k_\mp)\right.$$

$$+\int dk_{\pm}e^{ik_{\pm}z}\left(\frac{\omega^2}{c^2}-k_{\pm}^2-\mu_{11}^2\right)J_2(\mu_{11}r)e^{\pm i2\theta}b_{\pm 11}(k_{\pm})\Big]+c.c.$$

$$=4\pi\frac{\nu}{c}\delta(x)\delta(y)\frac{d}{dt}(x_c\pm iy_c). \tag{8}$$

There are two equations associated with (8). We multiply the equation with the upper sign by $\int_0^{2\pi}d\theta/2\pi\int_0^{r_g}J_o(\mu_{11}r)rdr$ and the equation with the lower sign by $\int_0^{2\pi}e^{i2\theta}d\theta/2\pi$ $\int_0^{r_g}J_2(\mu_{11}r)rdr$, then combine the results to pick out b_{-11}. Similarly, we multiply the equation with the upper sign by $\int_0^{2\pi}e^{-i2\theta}d\theta/2\pi\int_0^{r_g}J_2(\mu_{11}r)rdr$ and the equation with the lower sign by $\int_0^{2\pi}d\theta/2\pi\int_0^{r_g}J_o(\mu_{11}r)rdr$, then combine the results to pick out b_{+11}. The results are

$$e^{-i\omega t}\left[\int dk_{\mp}e^{ik_{\mp}z}\left(\frac{\omega^2}{c^2}-k_{\mp}^2-\mu_{11}^2\right)b_{\mp 11}(k_{\mp})\right]+\text{c.c.}=\frac{2\nu}{cI_{11}}\frac{m_oc^2}{e}\frac{d}{dt}(x_c\pm iy_c), \tag{9}$$

where $I_{11}=\mu_{11}^{-2}(\mu_{11}^2r_g^2-1)J_1^2(\mu_{11}r_g)$. Let

$$(x_c\pm iy_c)=\int dk_{\pm}\hat{\xi}_{\pm}(k_{\pm})e^{i(k_{\pm}z-\omega t)}+c.c.. \tag{10}$$

We substitute Eq. (10) into the wave equation, Eq. (9), to obtain a pair of equations that relate $b_{\mp 11}$ to $\hat{\xi}_{\pm}$. Keeping in mind that the variable of integration is a dummy variable in each case, we solve for b_{+11} and b_{-11}:

$$b_{\mp 11}(k)=-i\frac{2\nu}{cI_{11}}\frac{m_oc^2}{e}\frac{\omega-v_ok}{(\omega^2/c^2-k^2-\mu_{11}^2)}\hat{\xi}_{\pm}(k). \tag{11}$$

Next, we need to solve for the dependence of particle motion on the radiation field. We assume that $x^2+y^2\ll r_g^2$ such that the centroid motion depends only on the field on axis. The beam centroid equation of motion can be written as

$$\left(\frac{d^2}{dt^2}-k_s^2v_o^2\right)(x_c\pm iy_c)+\Omega_qk_qv_of(z)(x_c\mp iy_c)$$

$$=\frac{c}{\gamma_o}\left(\frac{\partial}{\partial t}+v_o\frac{\partial}{\partial z}\right)\left[(a_x\pm ia_y)|_{r=0}e^{-i\omega t}+c.c.\right], \tag{12}$$

where $k_s^2=2\nu/(\beta_o^2\gamma_o^3r_g^2)$, and $\Omega_q=eB_q/\gamma_om_oc$.

Returning to the quadrupole field, Eq. (1), let

$$f(z)=\sum_n f_n\cos(nk_qz). \tag{13}$$

For simplicity, we keep only the $n = 1$ term of the expansion. Substituting (7) and (10) into (12), we group terms with the same electromagnetic wave number k and evaluate the fields on axis. We solve for $\hat{\xi}_{\pm}$ in terms of $b_{\pm 11}$.

$$\left[-(\omega - v_o k)^2 - k_s^2 v_o^2\right] \hat{\xi}_{\pm}(k) + \Omega_q k_q (f_1/2) v_o \left[\hat{\xi}_{\mp}(k + k_q) + \hat{\xi}_{\mp}(k - k_q)\right]$$

$$= -i \frac{c}{\gamma_o} \frac{e}{m_o c^2} (\omega - v_o k) b_{\mp 11}(k). \tag{14}$$

We substitute (11) into (14), to obtain

$$S(\omega, k)\hat{\xi}_{\pm}(k) = -\frac{\Omega_q k_q f_1}{2 v_o} \left[\hat{\xi}_{\mp}(k + k_q) + \hat{\xi}_{\mp}(k - k_q)\right], \tag{15}$$

where

$$S(\omega, k) = (\omega/v_o - k)^2 \left(-1 + \frac{k_b^2}{(\omega^2/c^2 - k^2 - \mu_{11}^2)}\right) \tag{16}$$

and $k_b^2 = 2\nu/\gamma_o I_{11}$. Eliminating $\hat{\xi}_-$, we find that the longitudinal waveguide modes are coupled:

$$T_m(\omega, k)\hat{\xi}_+(k) = \frac{1}{2} K_d^4 \left[S_{m-1}\hat{\xi}_+(k + 2k_q) + S_{m+1}\hat{\xi}_+(k - 2k_q)\right], \tag{17}$$

where

$$S_m(\omega, k) = S(\omega, k + m k_q), \tag{18}$$

$$T_m(\omega, k) = S_{m-1} S_m S_{m+1} - \frac{1}{2} K_d^4 \left[S_{m-1} + S_{m+1}\right], \tag{19}$$

$K_d^2 = K_q k_q f_1/\sqrt{2}$ and $K_q = \Omega_q/v_o$.

From Eq. (17), the dispersion relation for the TE_{11} mode in the presence of the beam is a function of the determinant of an infinite tri-diagonal matrix of the form

$$det \begin{pmatrix} \ddots & \ddots & 0 & 0 & \dots \\ \ddots & T_{-2} & \frac{K_d^4}{2} S_{-3} & 0 & \dots \\ \dots & \frac{K_d^4}{2} S_{+1} & T_0 & \frac{K_d^4}{2} S_{-1} & \dots \\ \dots & 0 & \frac{K_d^4}{2} S_{+3} & T_{+2} & \ddots \\ \dots & 0 & 0 & \ddots & \ddots \end{pmatrix} = 0. \tag{20}$$

It can be shown from Eq. (20) that the growth rate of the instability is periodic in k. For a given unstable frequency ω_o, the unstable wave numbers are at all $k = k_0 + n k_q$,

where $n = 0, \pm 1, ...$ is an integer, and k_0 is the unstable wave number associated with a vacuum waveguide mode. Coupling to an infinite number of modes may be avoided in the approximation that

$$4\frac{K_d^8}{k_q^8} \ll 1. \tag{21}$$

It will be shown below that $2\frac{K_d}{k_q} < 1$ is required for phase stability. To zeroth order, the approximate dispersion relation is

$$T_0 = 0. \tag{22}$$

To first order, we find

$$det \begin{pmatrix} T_{-2} & \frac{K_d^4}{2} S_{-3} & 0 \\ \frac{K_d^4}{2} S_{+1} & T_0 & \frac{K_d^4}{2} S_{-1} \\ 0 & \frac{K_d^4}{2} S_{+3} & T_{+2} \end{pmatrix} = 0. \tag{23}$$

III. Analytical Beam Line Decomposition

Much insight can be obtained from analytical decomposition of the approximate dispersion relation, Eq. (22). This can give us analytical expressions for the growth rates and instability boundaries in parameter space.

The dispersion relation can be rewritten with the current coupling terms grouped together in a term $\bar{\sigma}$,

$$W_{-1}W_0W_{+1}\Pi_0 = \bar{\sigma}_0, \tag{24}$$

where

$$W_m(\omega,k) = (\omega/c)^2 - (k+mk_q)^2 - \mu_{11}^2, \tag{25}$$

$$\Pi_m(\omega,k) = \alpha_m^2\alpha_{m+1}^2\alpha_{m-1}^2 - \frac{K_d^4}{2}\left[\alpha_{m+1}^2 + \alpha_{m-1}^2\right], \tag{26}$$

$$\alpha_m(\omega,k) = \omega/v_o - (k+mk_q), \tag{27}$$

and

$$\begin{aligned}\bar{\sigma}_m = k_b^2\alpha_m^2\alpha_{m+1}^2\alpha_{m-1}^2[&W_{m+1}W_{m-1} + W_mW_{m-1} + W_mW_{m+1} \\ &-k_b^2(W_{m-1}+W_m+W_{m+1}) + k_b^4] \\ -\frac{1}{2}k_b^2K_d^4W_m&\left[\alpha_{m+1}^2W_{m-1} + \alpha_{m-1}^2W_{m+1}\right].\end{aligned} \tag{28}$$

The polynomial Π_0 can be rewritten as

$$\Pi_0(\omega,k) = (\alpha_0 - k_q)^2\Lambda_0 - 2k_qK_d^4\alpha_0, \tag{29}$$

where

$$\Lambda_0(\omega,k) = \left[\left(\alpha_0 + \frac{k_q}{2}\right)^2 - \left(\frac{k_q^2}{4} - K_d^2\right)\right]\left[\left(\alpha_0 + \frac{k_q}{2}\right)^2 - \left(\frac{k_q^2}{4} + K_d^2\right)\right]. \tag{30}$$

A good approximate beam mode decomposition can be obtained by dropping the last term of (29), since K_d^4/k_q^4 is typically much less than 1. There are six waveguide modes, i.e., $W_{-1}W_0W_{+1}$, and there are six beam modes. The four beam modes in (30) have the same characteristics as those in the helical quadrupole case.[2]

The beam line decomposition helps to define the approximate boundaries separating the orbit instability and the electromagnetic instability.

Orbit Instability

As in the helical quadrupole case, the electron beam develops orbit instability, when

$$k_q^2/4 < K_d^2, \tag{31}$$

with or without electromagnetic modes in a waveguide. This is confirmed by the numerical solution of the complete dispersion relation (23) and by particle simulations.

Electromagnetic Instability

Electromagnetic instability exists at the intersection of the

$$W_{-1}(\omega, k) = 0 \tag{32a}$$

waveguide mode and the

$$k + (-k_q/2 + \sqrt{k_q^2/4 - K_d^2}) - \omega/v_0 = 0 \tag{32b}$$

beam mode. This instability is repeated for all wave numbers, $k = k_0 \pm nk_q$, where $n = 0, \pm 1, \pm 2, ...$ When the intersection does not exist, we find that the beam is still unstable for

$$P \equiv \frac{k_q}{2} + \sqrt{\frac{k_q^2}{4} - K_d^2} < \sqrt{\frac{\mu_{11}^2}{\gamma_o^2 - 1}}, \tag{33}$$

but the growth rate is much smaller.

In the limit of zero beam current, a stability diagram based on Eqs. (31) and (33) is shown in Fig. 1

IV. Analytical Expressions for Growth Rates and Group Velocity

Following the same procedure as outlined in Ref. 2, analytical expressions for the spatial or temporal growth rates of the electromagnetic instability can be obtained. The derivation for the spatial growth rate is presented first. Electromagnetic instability occurs at a frequency and wavenumber, (ω_a, k_a), which satisfies (32a) and (32b), i.e., frequency ω_a satisfies

$$\sqrt{(\omega_a/c)^2 - \mu_{11}^2} + k_q = (\omega_a/v_0) + k_q/2 - \sqrt{k_q^2/4 - K_d^2}, \tag{34a}$$

and the corresponding wave number is

$$k_a = \sqrt{(\omega_a/c)^2 - \mu_{11}^2} + k_q. \tag{34b}$$

The derivation of the spatial growth rate is given below. The dispersion relation (24) can be rewritten as

$$\begin{aligned}&(k^2 - k_0^2)((k+k_q)^2 - k_0^2)((k-k_q)^2 - k_0^2)\\ &\left\{(k-k_2)^2[(k-k_4)^2 - \Delta k_1^2][(k-k_4)^2 - \Delta k_2^2] + 2k_q K_d^4 (k-k_1)\right\} = -\bar{\sigma}_0,\end{aligned} \tag{35}$$

where, at $\omega = \omega_a$,

$$\begin{aligned}\bar{\sigma}_0(k) \simeq & k_b^2 (k-k_1)^2 (k-k_2)^2 (k-k_3)^2 \left\{(k^2 - k_0^2)((k+k_q)^2 - k_0^2)\right.\\ & \left. - k_b^2[(k^2 - k_0^2) + ((k+k_q)^2 - k_0^2)]\right\}\\ & - \frac{k_b^2 K_d^4}{2}(k^2 - k_0^2)((k+k_q)^2 - k_0^2)(k-k_3)^2,\end{aligned} \tag{36}$$

$k_0 = \sqrt{(\omega/c)^2 - \mu_{11}^2}$, $k_1 = \omega/v_0$, $k_2 = (\omega/v_0) - k_q$, $k_3 = (\omega/v_0) + k_q$, $k_4 = (\omega/v_0) + k_q/2$, $\Delta k_1 = \sqrt{k_q^2/4 - K_d^2}$, and $\Delta k_2 = \sqrt{k_q^2/4 + K_d^2}$. Defining $k = k_0 + k_q + \delta k$, the imaginary part of δk is the spatial growth rate. Requiring $k_0 + k_q = k_4 - \Delta k_1$ and using the approximate beam modes (32b), the zeroth order dispersion relation (35) can be approximated by

$$p_a \delta k^2 + p_b \delta k + \sigma = 0, \tag{37a}$$

where

$$p_a = 4\Delta k_1 (\Delta k_2^2 - \Delta k_1^2) k_0 (k-k_2)^2 (k^2 - k_0^2)((k+k_q)^2 - k_0^2)|_{k=k_a, \omega=\omega_a}, \tag{37b}$$

$$p_b = 4k_q K_d^4 (k-k_1)k_0(k-k_2)^2(k^2-k_0^2)((k+k_q)^2-k_0^2)|_{k=k_a,\omega=\omega_a}, \qquad (37c)$$

and

$$\sigma = \bar{\sigma}_0|_{k=k_a,\omega=\omega_a}. \qquad (37d)$$

The derivation of (37a) assumed $\delta k \ll 2k_0$ and $\delta k \ll 2\Delta k_1$. The analytical growth rate expression evaluated at (ω_a, k_a) is

$$Im(\delta k) = \sqrt{(p_b/p_a)^2/4 - \sigma/p_a}. \qquad (38)$$

We can also give the analytical expression for the temporal growth rates. The dispersion relation (24) can be rewritten as

$$\frac{1}{c^6}(\omega^2-\omega_{-1}^2)(\omega^2-\omega_0^2)(\omega^2-\omega_1^2)$$

$$\left\{\frac{1}{c^6}(\omega-\omega_4)^2[(\omega-\omega_q)^2-\Delta\omega_1^2][(\omega-\omega_q)^2-\Delta\omega_2^2] - 2k_qK_d^4\frac{\beta_o^5}{c}(\omega-\omega_3)\right\} \simeq \beta_o^6\bar{\sigma}_0, \quad (39)$$

where, at $k = k_a$,

$$\begin{aligned}\bar{\sigma}_0(\omega) \simeq & \frac{k_b^2}{v_0^6}(\omega-\omega_2)^2(\omega-\omega_3)^2(\omega-\omega_4)^2\left\{\frac{1}{c^4}(\omega^2-\omega_1^2)(\omega^2-\omega_0^2)\right. \\ & \left. - \frac{k_b^2}{c^2}[(\omega^2-\omega_1^2)+(\omega^2-\omega_0^2)]\right\} \\ & - \frac{k_b^2K_d^4}{2c^4v_0^2}(\omega^2-\omega_1^2)(\omega^2-\omega_0^2)(\omega-\omega_2)^2,\end{aligned} \qquad (40)$$

$\omega_{-1} = \sqrt{(k-k_q)^2+\mu_{11}^2}c$, $\omega_0 = \sqrt{k^2+\mu_{11}^2}c$, $\omega_1 = \sqrt{(k+k_q)^2+\mu_{11}^2}c$, $\omega_2 = (k-k_q)v_0$, $\omega_3 = kv_0$, $\omega_4 = (k+k_q)v_0$, $\omega_q = (k-k_q/2)v_0$, $\Delta\omega_1 = \sqrt{k_q^2/4-K_d^2}v_0$, and $\Delta\omega_2 = \sqrt{k_q^2/4+K_d^2}v_0$. Defining $\omega = \omega_{-1}+\delta\omega$, the imaginary part of $\delta\omega$ is the temporal growth rate. Requiring $\omega_{-1} = \omega_q + \Delta\omega_1$, the analytical temporal growth rate expression can be simplified to

$$Im\left(\frac{\delta\omega}{c}\right) = \sqrt{q_b^2/4-q_c}\Big|_{\omega_{-1}=\omega_a,k=k_a}, \qquad (41a)$$

where

$$q_b = c^4\beta_o^5k_qK_d^4\left.\frac{(\omega-\omega_3)}{\Delta\omega_1(\Delta\omega_2^2-\Delta\omega_1^2)(\omega-\omega_4)^2}\right|_{\omega=\omega_{-1}}, \qquad (41b)$$

and

$$q_c = \left. \frac{c^{10}\beta_o^6 \bar{\sigma}_0}{4\Delta\omega_1(\Delta\omega_2^2 - \Delta\omega_1^2)\omega_{-1}(\omega - \omega_4)^2(\omega^2 - \omega_0^2)(\omega^2 - \omega_1^2)} \right|_{\omega=\omega_{-1}} . \tag{41c}$$

From our numerical solutions of the higher order dispersion relation (23) we conjecture that when a higher order dispersion relation, such as (23), is considered, spatial and temporal growth rates at other intersections in (ω, k) space of waveguide modes and other beam modes will collapse to expressions similar to Eqs. (35) and (41). (These intersection occur at $\omega = \omega_a$ and $k = k_a \pm nk_q$).

Because the beams have a finite length and because the group velocity of the instability is slower than the beam velocity, the instability can propagate out of the tail of the beam. From (38) and (41a), dropping the p_b and q_b terms, the group velocity of the instability is

$$v_g = \delta\omega/\delta k \simeq \left(\frac{\beta_o((\omega_a/c)^2 - \mu_{11}^2)^{1/2}}{\omega_a/c} \right)^{1/2} . \tag{42}$$

The number of e–folds, N, that can occur within a beam of length ℓ_b is

$$N = \min\left\{ \frac{L}{L_e}, \frac{\ell_b}{L_e(v_b - v_g)/v_b} \right\} \tag{43}$$

where $L_e = 1/\delta k$ is the e–folding distance, L is the total distance traveled by the beam and v_b is the beam velocity.

V. Numerical Examples

Here, the dispersion relations (22) and (23) are solved numerically. We verified that

i) Eq. (22) is a fair approximation to (23),

ii) the approximate beam mode decomposition Eq. (29) of (22) is good,

iii) the boundary of instability is as predicted by Eqs. (31) and (33) and

iv) analytical growth rate expressions are in good agreement with the results from (23).

Parameters for numerical examples are typical of a high-current, induction-accelerator beam, $I_e = 1\ kA$ and $\gamma_o = 5$. We chose a quadrupole gradient of $B_q k_q = 221$ G/cm, $f_1 = 4/\pi$, quadrupole wave number of $k_q = 0.5$ cm^{-1} and the waveguide radius of $r_g = 3\ cm$. These parameters fall in the electromagnetic unstable regime in Fig. 1, where $\sqrt{\mu_{11}^2/(\gamma_o^2 - 1)} = 0.125$ cm^{-1} and $P = 0.448$ cm^{-1} (see. Eq. (33)). Figure 2 plots the (ω, k) diagram corresponding to the zeroth order approximation to the dispersion relation, Eq. (22). The solid circle in Fig. 2 marks the instability denoted by Eqs. (32a,b). The instability encircled by the dashed curve is an erroneous one. It is modified when higher order expressions for the dispersion relation are solved. Figure 3 plots the first order approximation to the dispersion relation Eq. (23).

Figure 4 plots of the spatial growth rate as a function of wave number, k, for $\omega > 0$ from (23). The instability is periodic in k. The growth rates of all the instabilities are identical, except one. The instabilities at ($k \simeq k_0 - k_q$ and $k \simeq k_0 - 2k_q$) are from coupling to T_{+2}, where $k_0 \simeq 0.22$ cm^{-1}. The instabilities from coupling to T_{-2} (not shown) are at ($k \simeq k_0 + 2k_q$ and $k \simeq k_0 + 3k_q$). The instability at ($k \simeq k_0 - 2k_q$), similar to the instability marked by the dashed circle in Fig. 2, is erroneous, and is modified to give the same growth rate as that at $k_0 + k_q$ as more terms of the full determinant (20) are included.

Figure 5 plots the spatial growth rates as a function of frequency ω/c. for $\omega > 0$ for i) zeroth order approximation from Eq. (22), dashed (– – –) curve, ii) first order approximation from Eq. (23), solid (——) curve, iii) exact growth rates from Floquet formulation,[5] (+ symbols) and iv) analytic growth rate expression from Eq. (38), (•

symbols). The growth rate of the zeroth order approximation, the first order approximation and the Floquet formulation are in excellent agreement.

The unstable beam mode given by Eq. (32b) is in excellent agreement with the line in (ω, k) space in the dispersion diagram obtained by numerically solving the dispersion relation. Two of the six beam modes given by Eq. (29) are not as accurate. One of these two beam modes appears on the left-hand-side and one of these two beam modes appears on the right-hand-side of Fig. 2 Since the incorrect beam modes are not the unstable beam mode of interest and are sufficiently far from the unstable beam mode, the analytical growth rate expressions are in good agreement with the numerically obtained growth rates shown in Fig. 5.

Figures 6, 7, and 8 vary the quadrupole gradients while keeping all other parameters the same as that used for Fig. 2. Figure 6 compares the numerically (——) and analytically (•) obtained spatial growth rates for three different quadrupole gradients (a) $B_q k_q f_1 = 200$ G/cm, (b) $B_q k_q f_1 = 400$ G/cm and (c) $B_q k_q f_1 = 600$ G/cm. Figure 7 compares the numerically (——) and analytically (•) obtained temporal growth rates. The comparison of numerically obtained (hashed area) and analytically obtained (•) group velocities is shown in Fig. 8.

The boundaries of the instability regime predicted by Eqs. (31) and (33), in the limit of zero beam current, are in good agreement with numerically obtained boundaries.

Numerical verification of the weak unstable regime (V) was carried out by varying the energy of the electron beam while holding the rest of the parameters constant: quadrupole gradient of $B_q k_q f_1 = 200$ G/cm, quadrupole wave number of $k_q = 0.5$ cm^{-1}, the waveguide radius of $r_g = 1.5$ cm and current $I_e = 1$ kA. For $\gamma_o > 2.85$, the beam is in the unstable regime (I), while for $\gamma_o \leq 2.85$, the beam is in the unstable regime (V). The boundary for the instability is given by Eq. (33). Small growth rates are observed numerically for $\gamma_o \leq 2.85$ from the first order dispersion relation (23), (see Fig. 9).

For larger current and smaller quadrupole gradient, the difference of growth rates between regime (I) and (V) is much larger. Figure 10 is a plot of the temporal growth rates for different values of γ_o for the parameters: quadrupole gradient of $B_q k_q f_1 = 100$ G/cm, quadrupole wave number of $k_q = 0.5$ cm^{-1}, the waveguide radius of $r_g = 1.5$ cm

and current $I_e = 10$ kA.

In fact, instabilities at the intersection of unstable beam mode (32b) and all other waveguide modes also exist in the electromagnetic unstable region (I), except that their growth rate is much smaller, (see the small blip at $\omega/c \simeq 0.672$ of Fig. 5).

VI. Summary and Comments

Electromagnetic instability on an intense beam in a FODO lattice was studied by deriving and analyzing a dispersion relation, which is a matrix equation of infinite dimensions. We showed that numerical solutions of an appropriately truncated matrix equation give growth rates in excellent agreement with the exact growth rates as determined from Floquet Theory.[5]. Furthermore, analytical growth rates were obtained and are in good agreement with numerical solutions of the dispersion relation. Stability boundaries in parameter space were established and verified. The analysis will be extended to consider cases which include an additional nonzero axial (solenoidal) field.

The nature of the instability is such that growth should be observable for high current ($> 100A$), moderate energy ($\gamma < 100$) electron beams. Furthermore, the group velocity of the instability is slower than the beam velocity so that, in general, growth will not be observed in beam pulses of less than several nanoseconds for these parameters. For instance, this instability is not known to have been observed in rf linear accelerators, presumably because the growth rates are too small and/or the electron beam pulse length is short.

Ion beams are not expected to produce electromagnetic instabilities because ion beams are typically very slow, i.e., $\beta \leq 0.2$. The parameters of typical ion beam falls in the weak unstable regime of the instability diagram. Damping of the TE_{11} mode could easily be accomplished with finite Q values in the waveguide or the accelerator cavity.

Any high current induction driven electron accelerator utilizing FODO lattices would be susceptible to this instability under the idealized conditions stated here. Realistic effects, such as energy spread, nonlinear mode mixing, wave saturation may significantly reduce the effect of the instability.

Acknowledgments

This work was supported by the Defense Advanced Research Projects Agency, ARPA Order No. 7781, monitored by Naval Surface Warfare Center, and the Office of Naval Research. We would like to thank T. P. Hughes and D. Chernin for helpful discussions.

Appendix A: Proton or Ion Beams

For proton or ion beams, the coefficients of the dispersion relation are modified. We will consider ion beams with velocity v_i, mass m_i, charge per ion g and ion current $I_i = gev_i n_i(\pi r_b^2)$, where n_i is the ion density particle density and r_b is the ion beam radius. The complete dispersion relation is identical to Eq. (20), with the definitions of several constants replaced by those given here:

$$\Omega_q = \frac{ge}{\gamma m_i c} B_q, \tag{A.1}$$

$$K_q = \Omega_q / v_i, \tag{A.2}$$

$$\nu = \frac{g^2 e^2}{m_i c^2} n_i(\pi r_b^2) = \frac{geI_i}{m_i v_i c^2}, \tag{A.3}$$

and

$$k_b^2 = \frac{2}{I_{11}} \frac{\nu}{\gamma}. \tag{A.4}$$

Dominant instability exists if the beam mode

$$k + (-k_q/2 + \sqrt{k_q^2/4 - K_d^2}) - \omega/v_i = 0 \tag{A.5}$$

intersects the $W_{-1} = 0$ waveguide mode. Weak instabilities exist at intersections of (A.5) with other electromagnetic waveguide modes.

References

1. T. P. Hughes and B. B. Godfrey, Phys. Fluids **29**, 1698 (1986).
2. C. M. Tang, P. Sprangle, J. Krall, P. Serafim and F. Mako, Part. Accel., **35**, 101 (1991).
3. J. Krall, C. M. Tang, G. Joyce and P. Sprangle, Phys. Fluids B **3**, 204 (1991).
4. M. G. Tiefenback, S. D. Putnam, V. L. Bailey, Jr., J. P. Lidestri and J. A. Edighoffer, PSI Report PSIFR-2543-01 (1991); T. P. Hughes, T. C. Genomi, K. Nguyen and D. Welch, MRC Report MRC/ABQ-OR-1442 (1991).
5. T. P. Hughes and D. Chernin, submitted to Particle Accelerators.
6. C. M. Tang and J. Krall, submitted to the IEEE 1991 Particle Accel. Conf. Proc., May, 1991.

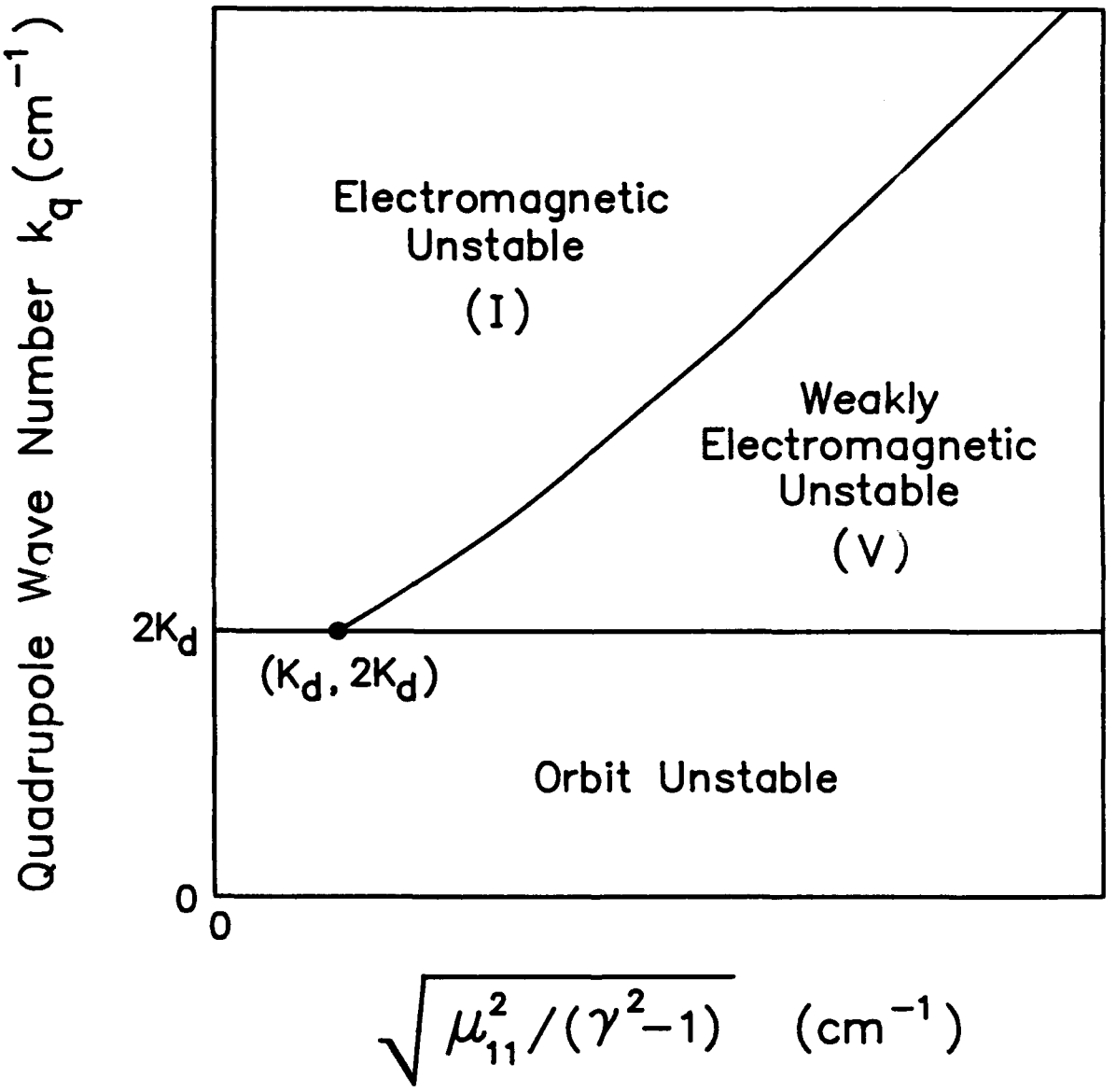

Fig. 1. Instability diagram in the limit of zero beam current.

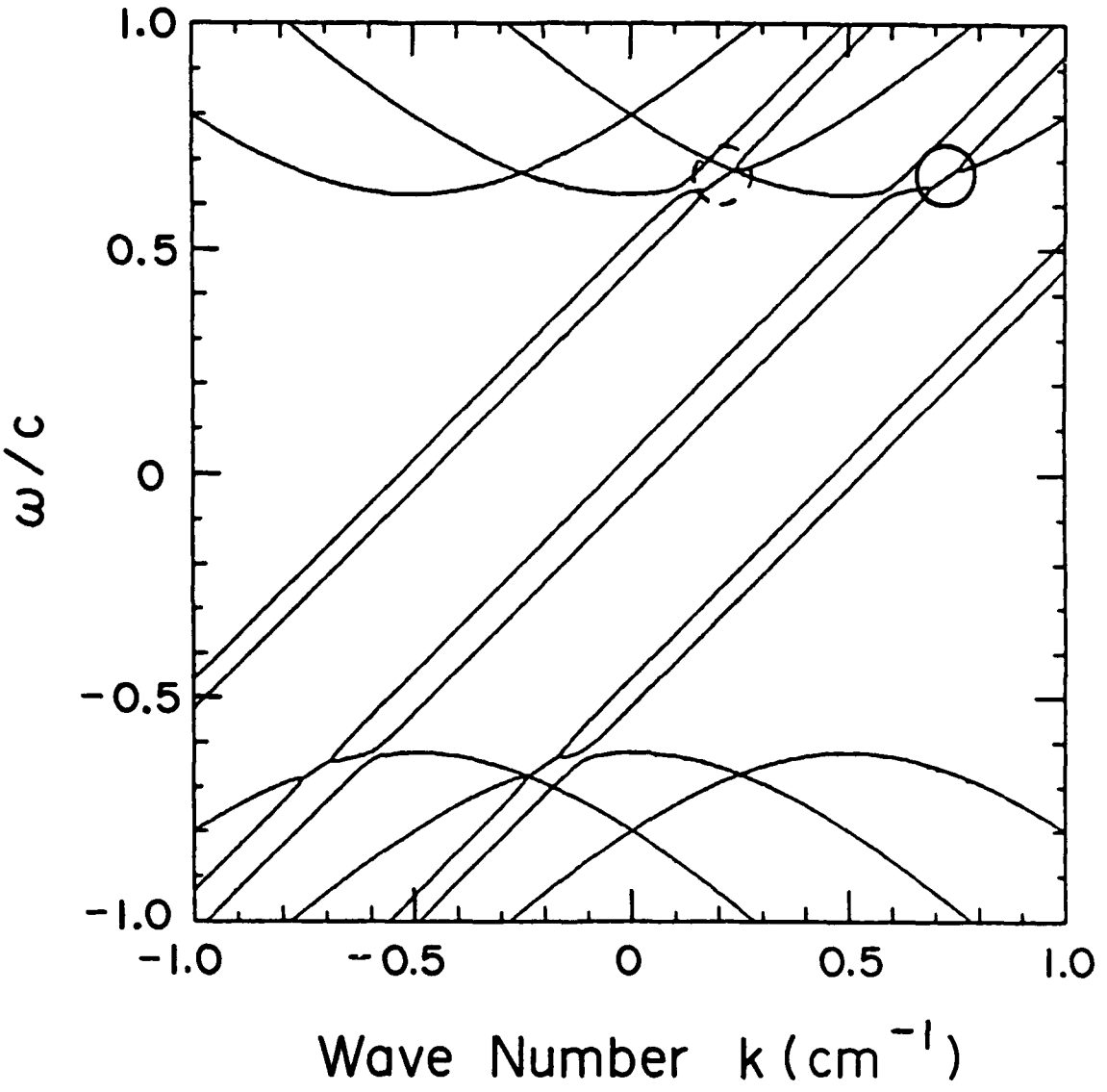

Fig. 2. Dispersion diagram of the zeroth order approximation of the dispersion relation Eq. (22).

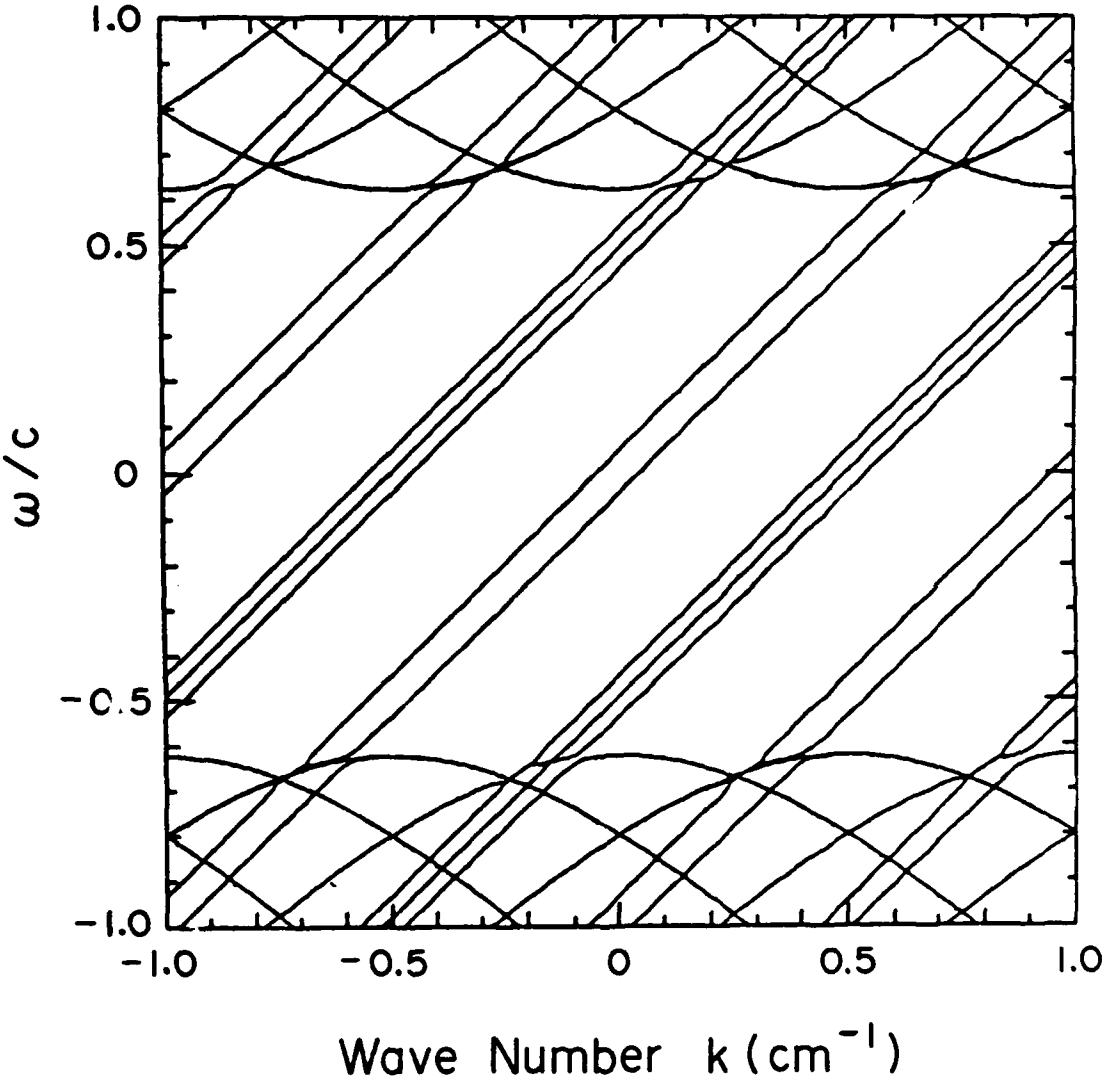

Fig. 3. Dispersion diagram of the first order approximation of the dispersion relation Eq. (23).

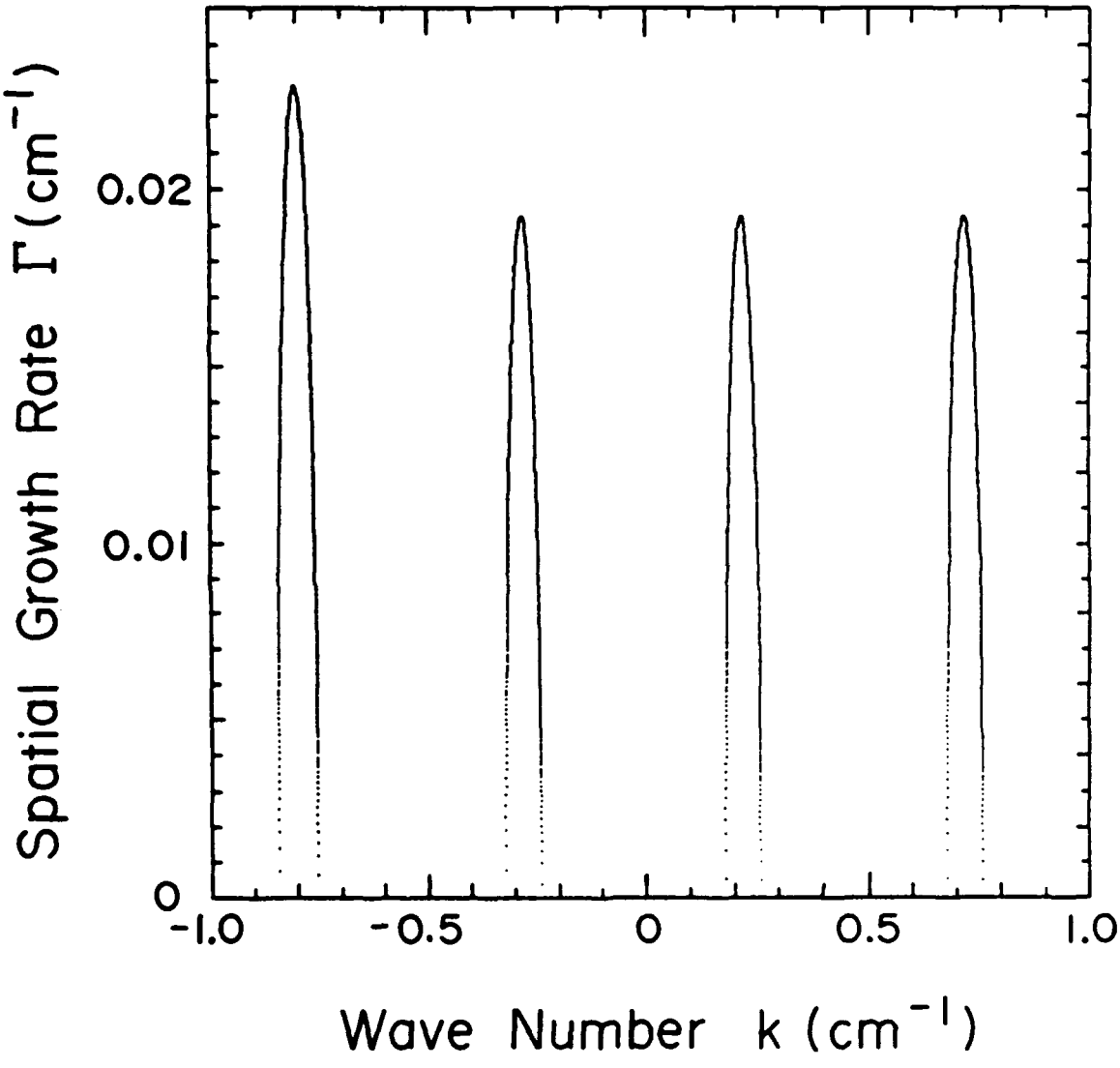

Fig. 4. Spatial growth rates for $\omega > 0$ as a function of wave number k.

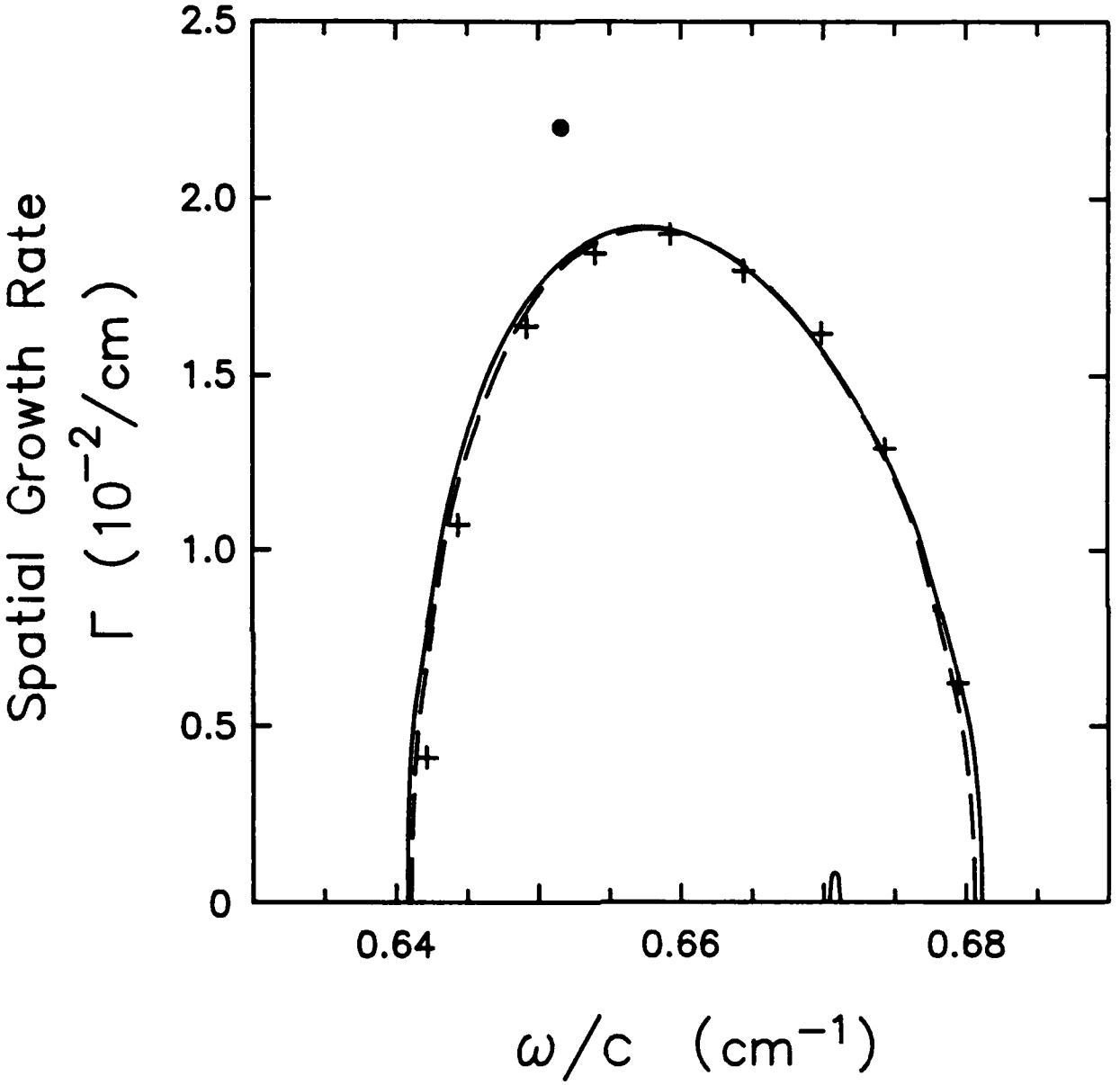

Fig. 5. Spatial growth rate as a function of frequency ω/c for i) zeroth order approximation, dashed (- - -) curve, ii) first order approximation, solid (——) curve, iii) exact growth rates from Floquet formulation, (+ symbols) and iv) analytic growth rate expression, (• symbols).

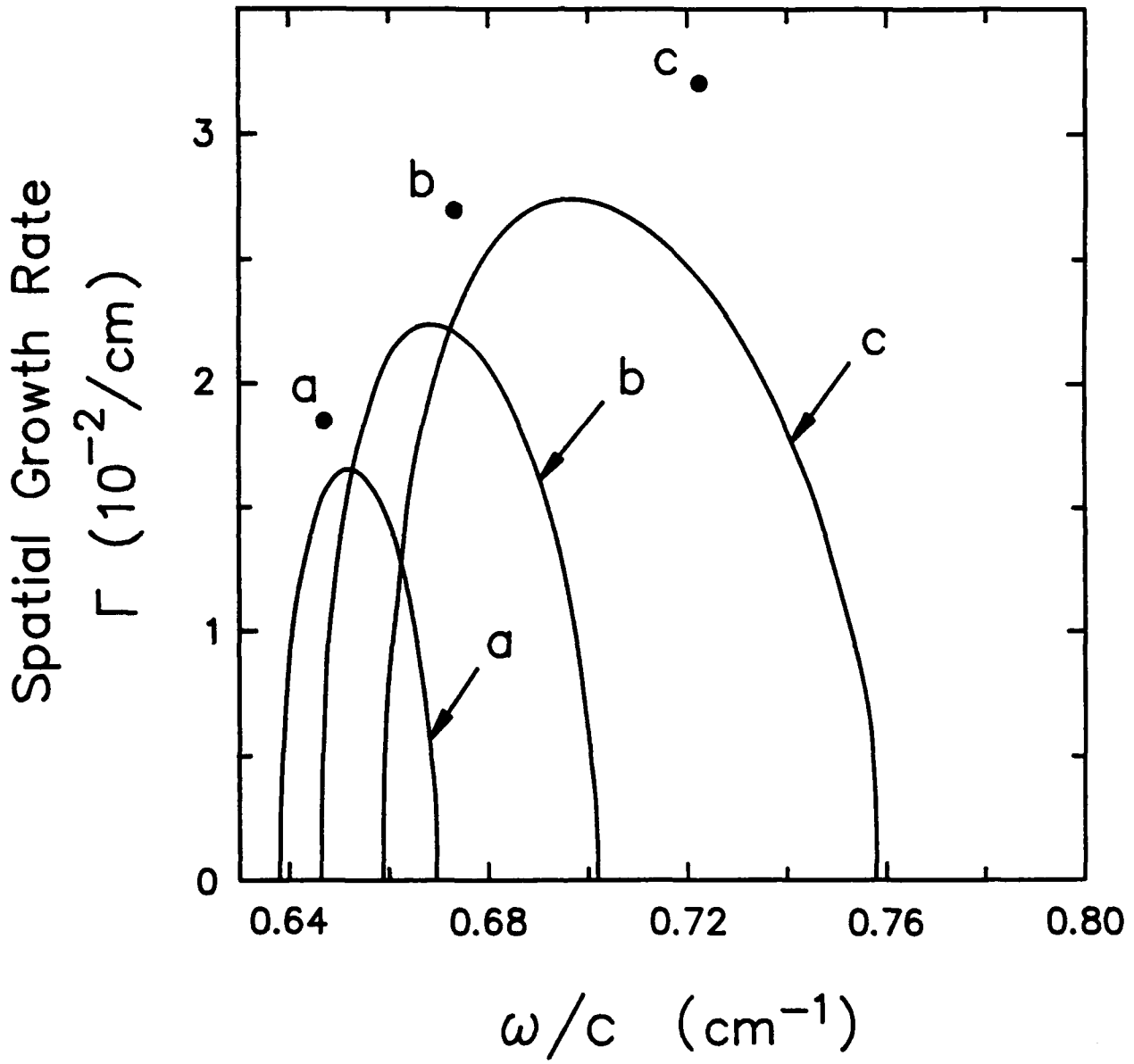

Fig. 6. Spatial growth rates for $\omega > 0$ and (a) $B_q k_q f_1 = 200$ G/cm, (b) $B_q k_q f_1 = 400$ G/cm and (c) $B_q k_q f_1 = 600$ G/cm, while keeping all the parameters the same as Fig. 2. The analytically calculated growth rates are indicated by (•).

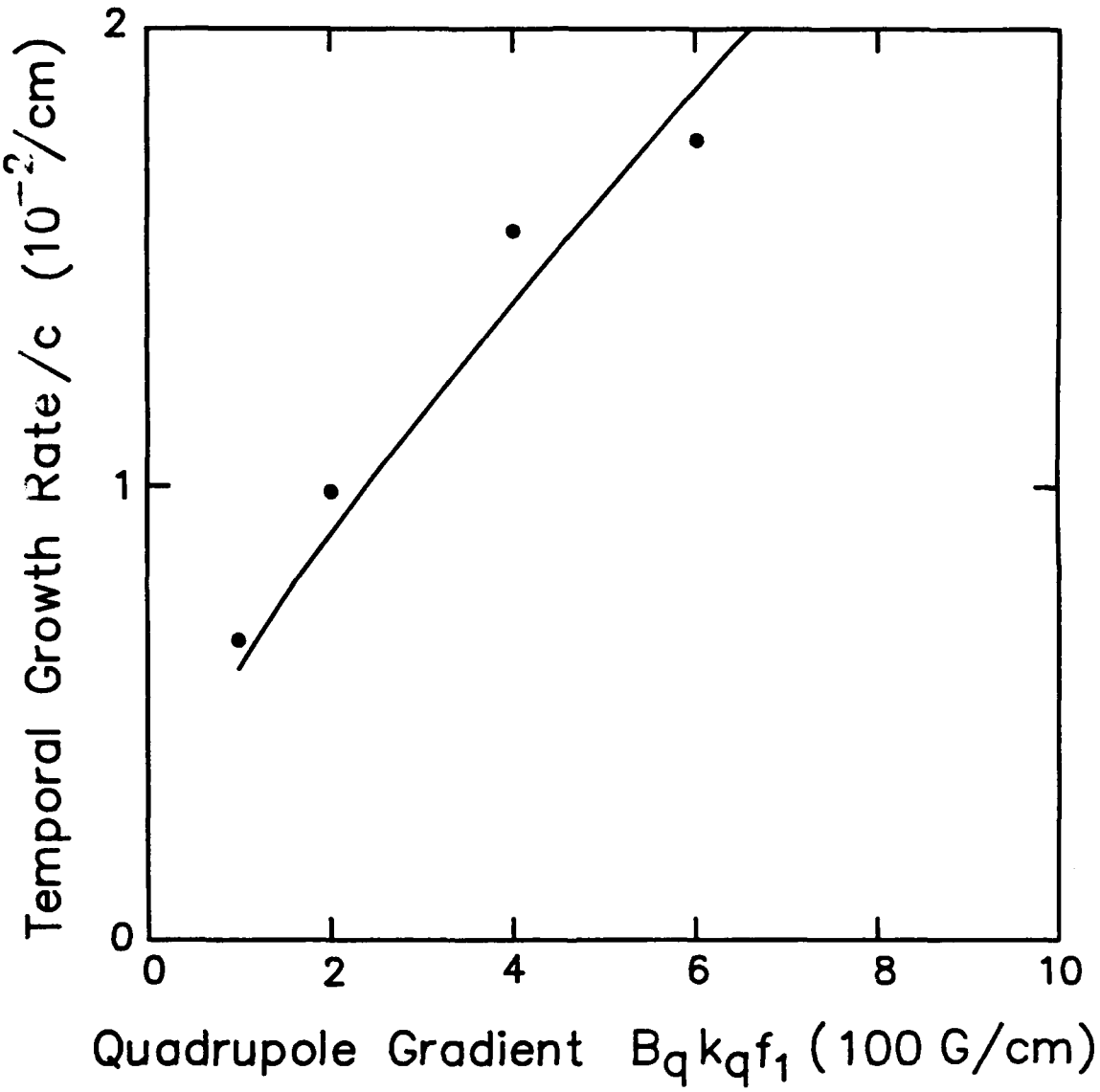

Fig. 7. Comparison of numerically (——) and analytically (•) obtained temporal growth rates for the same parameters as Fig. 6.

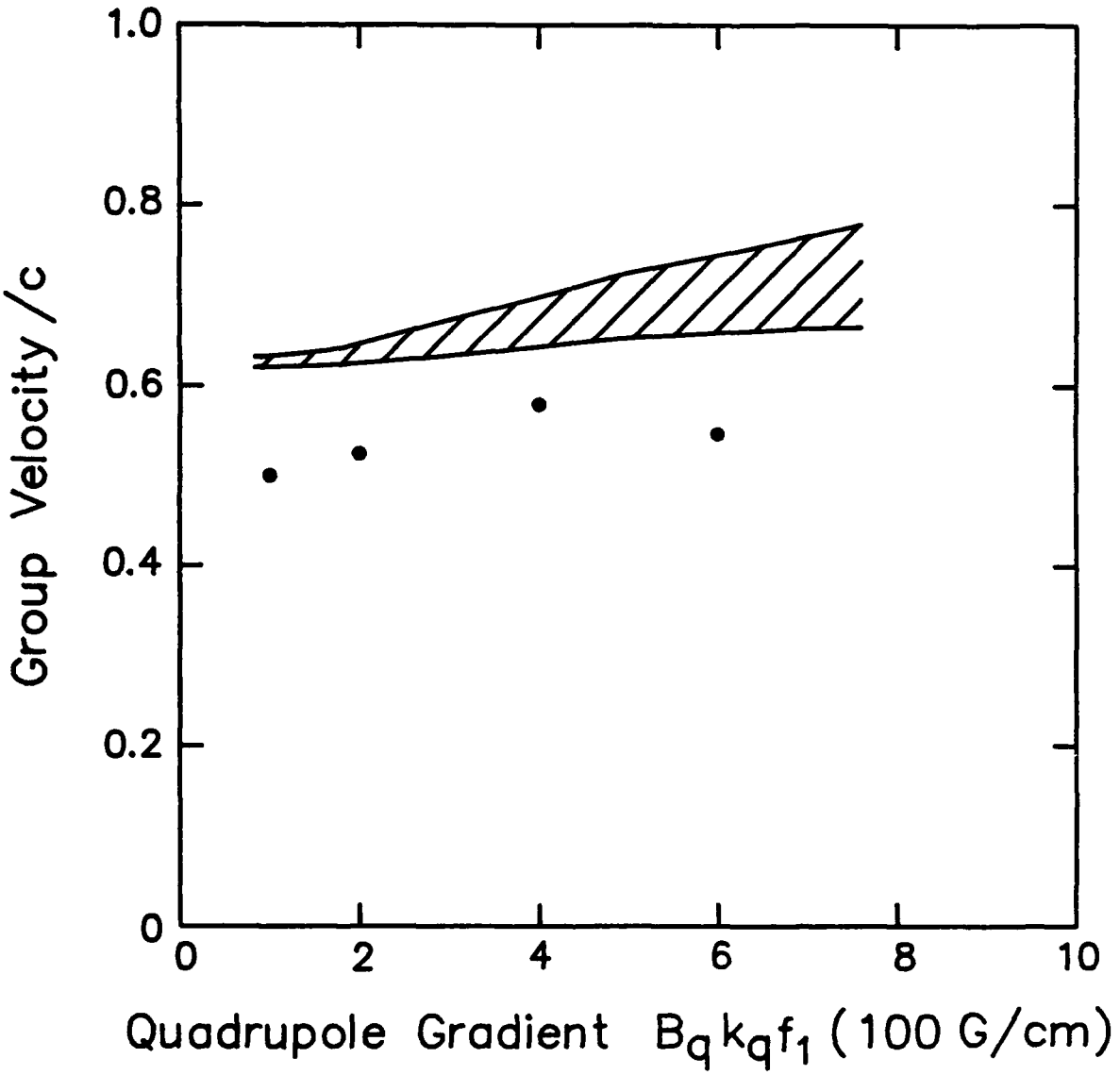

Fig. 8. The comparison of numerically obtained (hashed area) and analytically obtained (•) group velocities for the same parameters as Fig. 6.

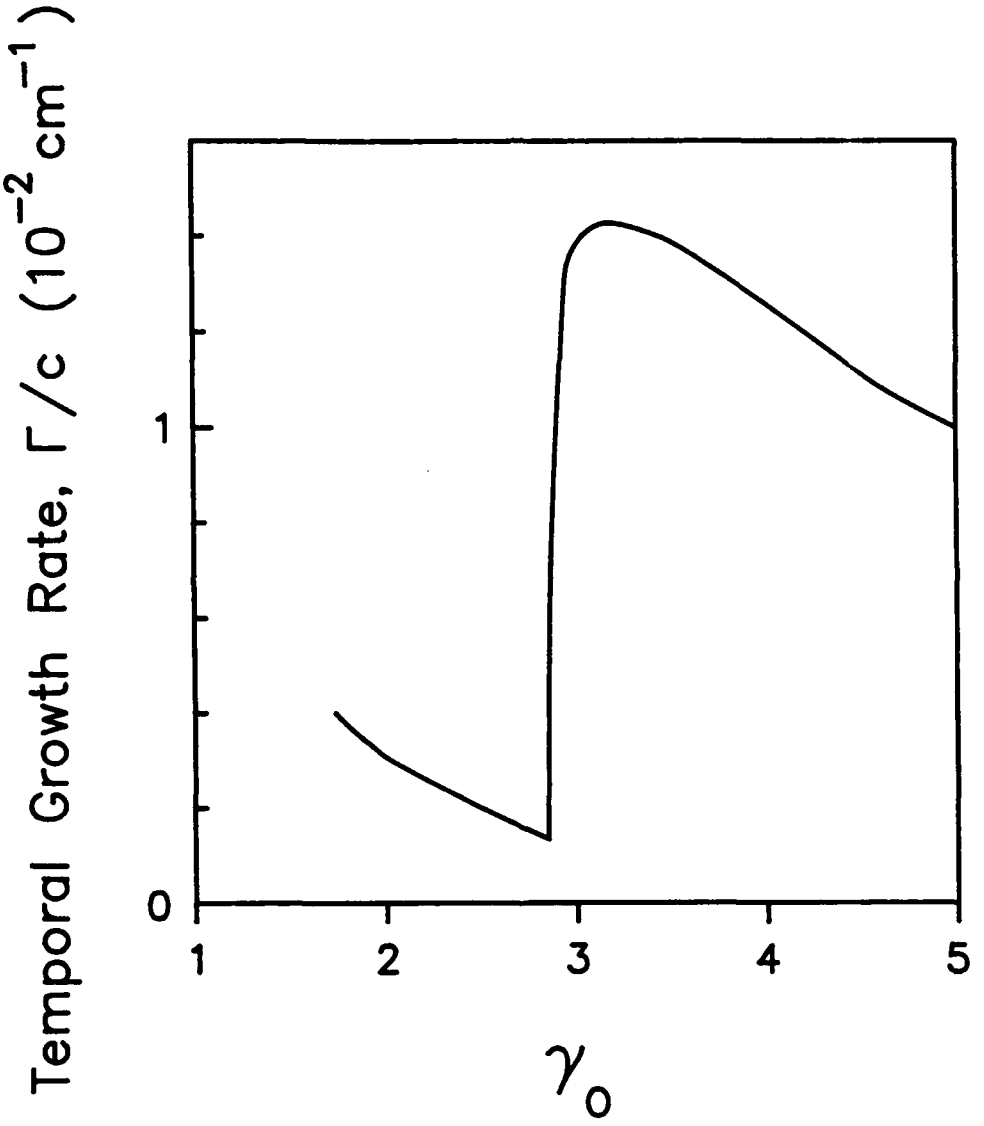

Fig. 9. Temporal growth rate versus γ_o for $B_q k_q f_1 = 200$ G/cm, $k_q = 0.5$ cm^{-1} $r_g = 1.5$ cm and $I_e = 1$ kA. The instability is in regime (I) for $\gamma_o > 2.85$ and in regime (V) for $\gamma_o \leq 2.85$.

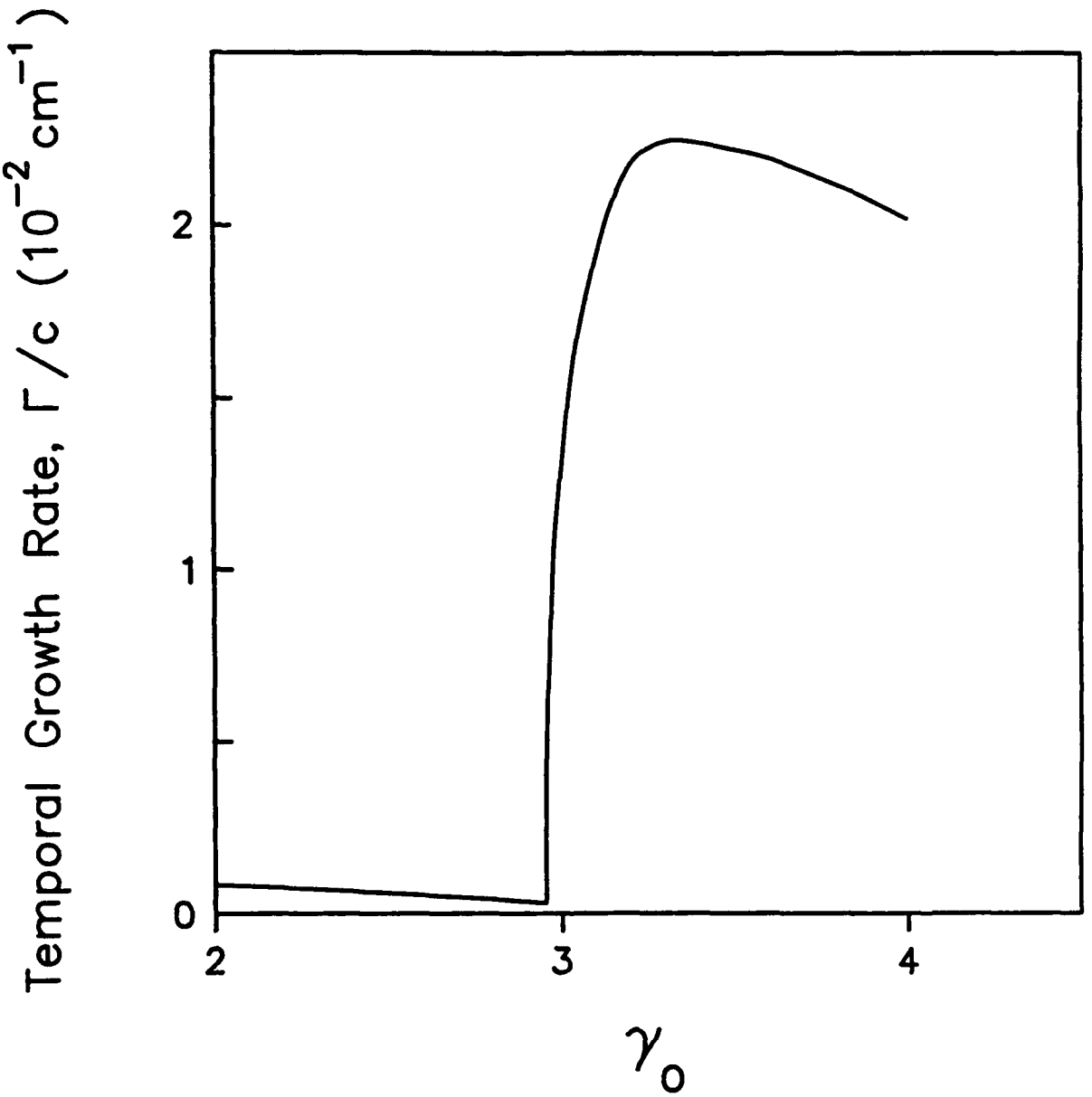

Fig. 10. Temporal growth rate versus γ_o for $B_q k_q f_1 = 100$ G/cm, $k_q = 0.5$ cm^{-1} $r_g = 1.5$ cm and $I_e = 10$ kA. The instability is in regime (I) for $\gamma_o > 2.9$ and in regime (V) for $\gamma_o \leq 2.9$.